

RESEARCH ARTICLE

Prolonged cadmium exposure alters benign uterine fibroid cell behavior, extracellular matrix components, and TGF β signaling

Yitang Yan¹ | Jingli Liu¹ | Arianna Lawrence¹ | Michael J. Dykstra² | Rick Fannin³ | Kevin Gerrish³ | Charles J. Tucker⁴ | Erica Scappini⁴ | Darlene Dixon¹ 

¹Molecular Pathogenesis Group, Mechanistic Toxicology Branch, Division of the National Toxicology Program (DNTP), National Institute of Environmental Health Sciences (NIEHS), NIH, Research Triangle Park, NC, USA

²Cellular & Molecular Pathogenesis Branch, DNTP, NIEHS, NIH, Research Triangle Park, NC, USA

³Signal Transduction Laboratory, Molecular Genomics Core Laboratory, NIEHS, NIH, Research Triangle Park, NC, USA

⁴Signal Transduction Laboratory, Fluorescence Microscopy and Imaging Center, NIEHS, NIH, Research Triangle Park, NC, USA

Correspondence

Darlene Dixon, Molecular Pathogenesis Group, Mechanistic Toxicology Branch, Division of the National Toxicology Program (DNTP), National Institute of Environmental Health Sciences (NIEHS), NIH, 111 TW Alexander Drive, P.O. Box 12233, Mail Drop B3-06, Research Triangle Park, NC 27709, USA.
 Email: dixon@niehs.nih.gov

Funding information

HHS | NIH | National Institute of Environmental Health Sciences (NIEHS), Grant/Award Number: ES021196-27

Abstract

The heavy metal Cadmium (Cd), a widespread environmental contaminant, poses serious hazards to human health and is considered a metalloestrogen and carcinogen. In women with uterine fibroids, there is a significant association between blood Cd levels and increased fibroid tumor size. The aim of this study was to determine if benign human uterine leiomyoma (fibroid) cells could be malignantly transformed *in vitro* by continuous Cd exposure and, if so, explore a molecular mechanism by which this could occur. We found when fibroid cells were exposed to 10 μ M CdCl₂ for 8 weeks, a robust and fast-growing Cd-Resistant Leiomyoma (CR-LM) cell culture was established. The CR-LM cells formed viable colonies in soft agar and had increased cytoplasmic glycogen aggregates, enhanced cell motility, a higher percentage of cells in G2/M phase, and increased expression of the proliferation marker Ki-67. NanoString analysis showed downregulation of genes encoding for extracellular matrix (ECM) components, such as collagens, fibronectins, laminins, and SLRP family proteins, whereas genes involved in ECM degradation (MMP1, MMP3, and MMP10) were significantly upregulated. A volcano plot showed that the top differentially genes favored cancer progression. Functional analysis by ingenuity pathway analysis predicted a significant inhibition of TGF β 1 signaling, leading to enhanced proliferation and attenuated fibrosis. Prolonged Cd exposure altered phenotypic characteristics and dysregulated genes in fibroid cells predictive of progression towards a cancer phenotype. Therefore, continuous Cd exposure alters the benign characteristics of fibroid cells *in vitro*, and Cd exposure could possibly pose a health hazard for women with uterine fibroids.

Abbreviations: AIG, anchorage-independent growth; BGN, biglycan; CR-LM, cadmium resistant leiomyoma; DCN, decorin; DEG, differentially expressed genes; ECM, extracellular matrix; FMOD, fibromodulin; Ht-UtLM, human uterine leiomyoma cell line immortalized via retroviral transfection of telomerase; IPA, ingenuity pathway analysis; Ki-67, antigen Ki-67 identified by monoclonal antibody Ki-67; LUM, lumican; MMP1, matrix metalloproteinase 1; PTGS2, prostaglandin-endoperoxide synthase 2; SLRP, small leucine-rich proteoglycans; SMAD3, SMAD family member 3; SPP1, secreted phosphoprotein 1; SULF1, sulfatase 1; TGF β 1, transforming growth factor beta 1; THBS1, thrombospondin 1; VEGFA, vascular endothelial growth factor A.

This is an open access article under the terms of the Creative Commons Attribution-NonCommercial-NoDerivs License, which permits use and distribution in any medium, provided the original work is properly cited, the use is non-commercial and no modifications or adaptations are made.

Published 2021. This article is a U.S. Government work and is in the public domain in the USA. *The FASEB Journal* published by Wiley Periodicals, Inc. on behalf of Federation of American Societies for Experimental Biology.

KEYWORDS

cadmium, extracellular matrix, metalloestrogen, NanoString, proliferation, TGF β 1 signaling, uterine fibroid cells, uterine leiomyoma

1 | INTRODUCTION

Uterine fibroids (leiomyomas) are common benign smooth muscle neoplasms of the uterus. Fibroids have both smooth muscle and extracellular matrix (ECM) components that contribute to a substantial amount of fibrous matrix in many tumors, hence the colloquial term, “fibroid.” Uterine fibroids cause symptoms such as uterine bleeding and pelvic pain that can be severe resulting in infertility or major surgery.¹ Fibroid risk is associated with race, with Black women having a higher incidence of developing fibroids earlier in life.² Fibroids do not generally occur before menarche, and they shrink dramatically after menopause. Because fibroids are hormonally regulated, it has been suggested that exposure to exogenous estrogens and metalloestrogens, such as Cd, may contribute to fibroid growth.¹ In occupational settings, workers may be exposed to Cd in activities such as smelting, zinc refining, electroplating, and welding. In nonoccupational settings, Cd exposure typically results from tobacco consumption and ingestion of contaminated foods and drinking water. Chronic exposure to Cd, such as cigarette smoke, is thought to contribute to cancer development, and epidemiological studies show causal associations between Cd exposure and the risk of prostate, breast, and lung cancer.³ In human tissues, Cd concentrations have been reported to range from 0.8 μM to up to 1700 μM depending on age, duration of exposure, environmental exposure concentration, occupation, sex, and smoking status.⁴⁻⁶ Additionally, Cd bioaccumulates in many tissues with a half-life of approximately 10-30 years.^{7,8}

It is thought that Cd may mimic the effects of estrogen and contribute to endocrine disruption of the reproductive systems of wildlife and to the high incidence of hormonally related cancers and diseases observed in human populations.⁹ Previous studies have shown that Cd acts like steroidal estrogens *in vitro* in breast cancer cells due to its ability to form a high-affinity complex with the hormone binding domain of the classical estrogen receptor alpha (ESR1).¹⁰⁻¹² We have found that Cd can act as a metalloestrogen by nongenomic mechanisms upregulating membrane-associated G protein-coupled estrogen receptor 1 (GPER1) and epidermal growth factor receptor (EGFR), and stimulating proliferation of hormonally responsive human uterine leiomyoma cells.^{13,14} We have also shown that in human uterine leiomyoma cells exposed to Cd at concentrations of 10^{-4} to 200 μM , significant proliferative effects were observed at doses of 0.1 to 20 μM at 24, 48, and 72 hours.¹³

An evolving body of evidence supports that Cd may be associated with multiple adverse outcomes in women's reproductive health.¹⁵ The correlation between uterine fibroid volume and blood heavy metal concentrations was investigated, and it was found that blood Cd concentrations correlated with fibroid volume.¹ In this study, we examined the effects of chronic Cd exposure on fibroid cells to determine if Cd could induce phenotypic and signaling pathway alterations that would suggest possible cancer progression. Our results indicate that prolonged Cd exposure may pose a carcinogenic hazard for women with uterine fibroids and may have important clinical implications.

2 | MATERIALS AND METHODS

2.1 | Cell cultures

A human uterine leiomyoma cell line immortalized via retroviral transfection of telomerase (ht-UtLM) was generated by our laboratory and maintained in medium as previously described.¹⁶ Human fibroblast and vulvar leiomyosarcoma (SK-LMS-1) cell lines were cultured in DMEM medium supplemented with 10% FBS. All cultures were kept in a standard tissue culture incubator at 37°C with 5% CO₂.

2.2 | Cadmium treatment

For 1-week Cd exposure, ht-UtLM cultures were maintained in the culture medium¹⁶ supplemented with 10 μM CdCl₂ for 1 week with fresh medium replacement on day 3. For 8-week Cd-exposure, the ht-UtLM cultures were maintained continuously in ht-UtLM culture medium supplemented with 10 μM CdCl₂ for 8 weeks. The culture medium was replaced with fresh medium every 3 days. Passage-matched control ht-UtLM cultures were run concurrently with Cd exposed cells. All data assessments were done following 8 weeks of continuous Cd exposure using the Cd exposure protocol described above.

2.3 | RNA isolation and NanoString transcriptional profiling

Total RNA was isolated from three RNA samples from three independent experiments for control and Cd-exposed leiomyoma cells by extracting with Trizol Reagent (ThermoFisher

Cat# 15596026) and subsequently purifying with RNeasy Mini kit (Qiagen Cat#74104). The mRNA expression was examined using the NanoString platform with Cancer Progression (NS_Cancerprog_C4972) and Cancer Pathways (NS_CancerPath_C2535) panels. For both codesets, RNA expression was quantified on the nCounter Digital Analyzer, and the counts were generated with nSolver (v4.0) software. Data were adjusted utilizing the manufacturer's positive and negative control probes, as well as internal house-keeping genes which had the lowest variability across all samples. The nSolver adjusted data were then imported into Partek (v7.0), log₂ transformed and quantile normalized.

2.4 | Ki-67 antibody staining and quantification

Approximately 3.0 mL of ht-UtLM and CR-LM cell cultures (about 75 000 cells) were inoculated into chamber slides (ThermoFisher Scientific, Lab-Tek Flaskette Chamber Slide system, Cat# 177453) and grown to 80% confluency in Cd-free culture medium. The slides were fixed in 4% paraformaldehyde in PBS for 10 minutes, rinsed with 1× automation buffer (Biocare Medical Cat# TWB945M), permeabilized in 0.2% Triton X-100, and washed in 1× automation buffer. Rabbit polyclonal anti-Ki67 (Biocare Medical Cat#CRM325) antibody was applied to the slides at a dilution of 1:100 for 30 minutes. The slides were then incubated with anti-Rabbit IgG HRP Polymer (BioCare Medical #MP-7401) for 30 minutes. The slides were then treated with 3,3-diaminobenzidine to develop chromogenic reaction. Slides were counterstained with hematoxylin and scanned with Leica Aperio AT2 Digital Whole Slide Scanning system. Three slides for each treatment group were prepared and quantified.

2.5 | Immunofluorescence staining

The ht-UtLM and CR-LM cells were stained with COL1A1 (E6A8E) Rabbit mAb (Cell Signaling Cat# 39952) and Fibronectin (EP5) mAb (Sana Cruz Biotechnology Cat# sc-8422). The procedure for immunofluorescence staining and confocal microscopy observations was done as described previously.¹⁷ Three slides were stained and evaluated per study group.

2.6 | Transmission electron microscopy

The sample cells were detached with 0.25% trypsin solution, resuspended in 1× PBS and centrifuged at 1000 rpm. The pellets were fixed in 4F:1G fixative¹⁸ and submitted to NIEHS EM core for processing, and the detailed procedure for sample processing was described previously.¹⁹ Digital images were

captured with a Gatan Orius SC1000/SC600 attached to a FEICO Tecnai T12 transmission electron microscope. Three independent blocks were prepared and evaluated by electron microscopy for each group of control and Cd-treated cells.

2.7 | Cell migration tracking

The CR-LM and control cells were grown in glass bottom microwell dishes (MatTek Corporation, Ashland, MA, USA, Part No# P35G-1.5-14-C) for 72 hours to reach about 80% confluency in the Cd-free culture medium and stained with 1:10 000 dilution of Hoechst 33342 for 2 hours. The time-lapse images in 3 × 3 tiles were recorded with Zeiss LSM 880 confocal microscope (objective Zeiss Plan-Apochromate 20X/0.8 M27). The time interval was set at 5 minutes, and a total of 100 frames were recorded. The tracking lengths for individual nuclei were calculated by autoregressive motion algorithm by IMARIS. The track length histograms were produced by GraphPad PRISM 8, and the probability density distribution was produced by RStudio.

2.8 | Cell cycle analysis

The sample cells were fixed with cold 70% ethanol overnight. Prior to analysis with BD LSRFortessa flow cytometer, the samples were stained with 1.0 mL Propidium Iodide solution (20 µg PI/mL, 10 units/mL RNase ONE Ribonuclease in 1× PBS) for 30 minutes in dark. To ensure that the samples were free from cell aggregates that may block the cytometer, the stained samples were filtered in a Falcon tube (5 mL Polystyrene Round-bottom Tube with Cell-Strainer Cap, Falcon Cat# 352235), collected at least 10 000 cells in a LO flow rate, and the data were analyzed by ModFit LT. Three independent samples were prepared for control and CR-LM groups under conditions of normal (20% serum), starvation (cultured in serum-free medium for 48 hours), and resupplemented (added 20% serum to the culture medium for 24 hours).

2.9 | Soft agar assay

Tissue culture 6-well plates (BECTON DICKINSON Cat# 353046) were used for soft agar assays. In each well, 1.5 mL 0.5% noble agar containing 1× MEM and 10% FBS was used to serve as the bed agar. The sample cells to be tested in the amount of 5×10^4 cells per well were seeded into 1.5 mL 0.3% noble agar containing MEM and 10% FBS on top of the bed agar. Three weeks later, the plates were stained overnight with 0.05% vital stain (P-Iodonitrotetrazolium Violet, Sigma Cat# I-8377) and imaged with inverted epifluorescence microscope. Six wells were setup for each cell type evaluated.

2.10 | nSolver analysis

We imported RCC and RLF files to nSolver 4.0 for each panel and built a MultiRLF experiment that combined the data from the two panels and normalized the data with overlapping probes. The Box Plot graphs were exported from MultiRLF experiment. The volcano plot was generated by differential expression module with Bejamini–Hochberg correction and modified with RStudio for better readability.

2.11 | Ingenuity pathway analysis

The NanoString dataset containing gene identifiers and corresponding expression values was uploaded into ingenuity pathway analysis (IPA). A fold-change cutoff of 2.0 was set to identify molecules whose expression was significantly differentially expressed. Right-tailed Fisher's exact test was used to calculate a p-value determining the probability that each biological function assigned to that network due to chance alone (Krämer A., et. al., 2014).

2.12 | Matrix metalloproteinases protein array

The cells were lysed with cold lysis buffer (150 mM NaCl, 0.5% Triton X-100, 0.05% Na deoxycholate, 4% glycerol, 1 mM DTT, 10 mM Tris-HCl, pH 7.4) supplemented with protease inhibitor cocktail (Roche Life Science, Indianapolis, IN, Cat# 11836153001). The proteomic profile of the matrix metalloproteinases (MMP) was produced with RayBio C-Series Human Matrix Metalloproteinase Antibody Array C1 (RayBiotech Cat# AAH-MMP-1-8).

2.13 | TGFB phospho antibody array

TGFB phospho antibody array (Full Moon Biosystems, Cat# PTG176), which includes 176 antibodies with six replicates for each antibody, was used to analyze the Cd treated and control samples. The proteins were extracted with Antibody Assay Kit (Full Moon Biosystems, Cat# KAS02). The lysates were purified and labeled by biotin, and then combined with antibodies in the array. The slides were scanned by Agilent Technologies Microarray scanner.

2.14 | Statistical analysis

The statistical significance of the differences was determined by t-test (one-tailed distribution, two-sample unequal variance). Statistical significance was defined as $P < .05$.

3 | RESULTS

3.1 | Cd exposure altered cell morphology and ultrastructure

The control ht-UtLM cells were typically elongated (Figure 1A); however, upon exposure to 10 μ M Cd for 7 days, many of the cells had lost their typical elongated morphology. Beneath masses of floating spherical cells, there were a few elongated cells that remained tightly attached (Figure 1B). Interestingly, by 8 weeks, Cd exposure at 10 μ M resulted in the formation of robust Cd-Resistant ht-UtLM (CR-LM) cultures with focal cellular aggregates (Figure 1C). As shown in Figure 1D, the nuclei of control cells were intact and oval-shaped, with a relatively smooth nuclear surface. However, the nuclei of 7-day Cd-treated cells had pitted surfaces, some with multiple lobulations, indicating significant cellular and nuclear damage (Figure 1E). However, at 8 weeks, Cd-exposed cells had smooth nuclear surfaces with no evidence of cellular damage (Figure 1F). Ultrastructurally, CR-LM showed large deposits of glycogen granules at the periphery of the cells compared with ht-UtLM cells (Figure 1G-J).

3.2 | Cd exposure increased Ki-67 expression and promoted cell cycle progression

To evaluate cell proliferation, cell cycle progression and expression of the proliferation marker, Ki-67, were assessed. As shown in Figure 2, there was a higher percentage of Ki-67 negative cells (with blue nuclei) in the control (Figure 2A,B), whereas CR-LM cells had fewer Ki-67 negative nuclei (Figure 2C,D). Further automated counting of the nuclei with Imaris showed that in the control population, the average percentage of Ki-67 negative cells (G_0 quiescent phase) was 37.9%. In contrast, the average percentage of Ki-67 negative cells in CR-LM was 4.8% (Figure 2E). Therefore, prolonged Cd exposure effectively decreased the percentage of quiescent cells by 7.9-fold (37.9%/4.8%; $P < .001$) and rendered CR-LM cells to be mostly in active phases of the cell cycle. To determine DNA synthesis dynamics, we conducted cell cycle analysis with flow cytometry. The CR-LM culture had a significantly higher ($P < .001$) percentage of cells in G2/M phases (8.8%) versus controls (3.4%) when cultured in normal medium (Figure 2F). Under serum starvation conditions for 48 hours, the percentage of G2/M cells in CR-LM were 3.4-fold greater ($P < .001$) than the ht-UtLM controls (Figure 2F). Specifically, after serum resupplementation for 24 hours, the percentage of cells in S phase from CR-LM (51.5%) was significantly greater ($P < .01$) than the control (35.3%) (Figure 2F).

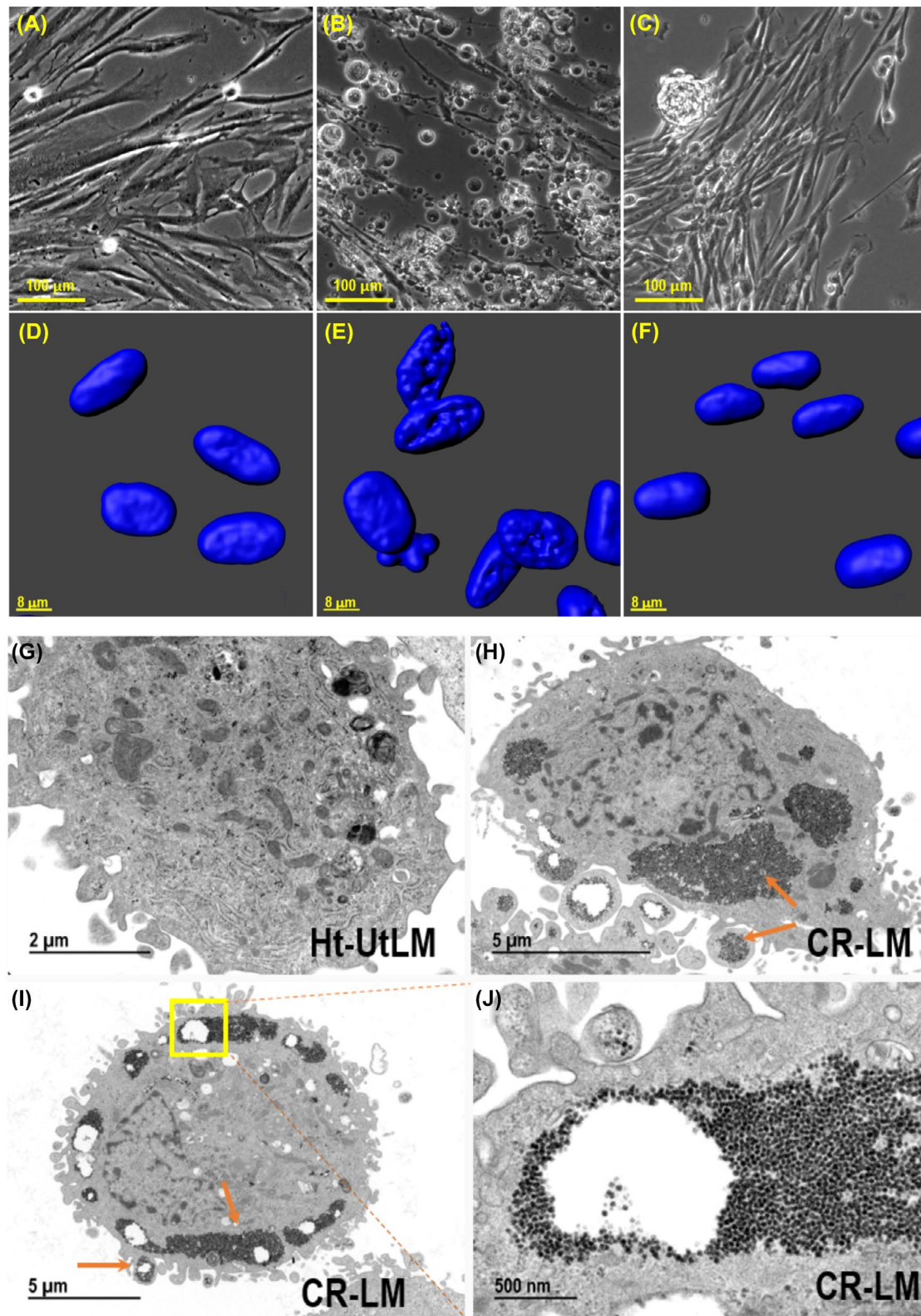


FIGURE 1 The effects of 10 μM Cd exposure on ht-UtLM cells and ultrastructural characteristics of ht-UtLM and 8-week Cd-exposed ht-UtLM cells (designated CR-LM). A, No Cd exposure; (B) Cd exposure for 1 week. (C) Cd exposure for 8 weeks. Bottom row: The Z-stack images acquired with Zeiss LSM 880 confocal microscope, DAPI signal only. D, No Cd exposure; (E) Cd exposure for 1 week; (F) Cd exposure for 8 weeks. Ultrastructural images: (G) Ht-UtLM cell; (H) CR-LM cell; note the peripheral cytoplasmic accumulations of glycogen; (I) CR-LM cell; (J) Higher magnification of region in box shown in panel (I). A–C (scale bar = 100 μm); D–F (scale bar = 8 μm); G (scale bar = 2 μm); H and I (scale bar = 5 μm); J (scale bar = 500 nm)

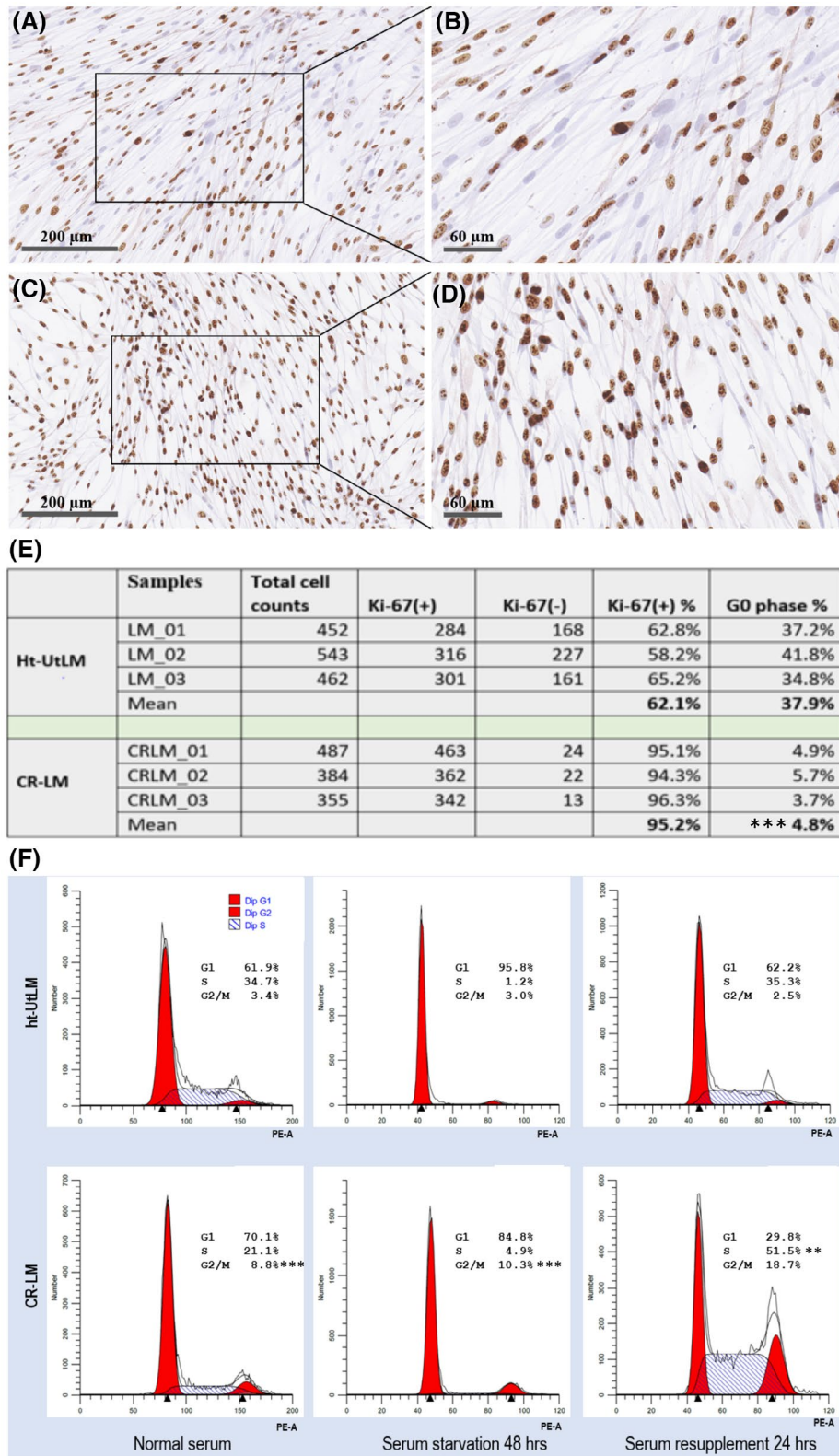


FIGURE 2 Prolonged Cd exposure stimulated Ki-67 expression and cell cycle progression. A and B, Ht-UtLM cells. C and D, CR-LM. E, Quantification of Ki-67 positive and negative cells. The difference in Ki-67 positive cells between the groups was statistically significant ($***P < .001$). F, Prolonged Cd exposure promoted higher percentages of CR-LM cells in the G2/M phase of the cell cycle compared with ht-UtLM cells as analyzed by flow cytometry under normal and serum starvation conditions ($***P < .001$). After serum resupplementation for 24 hours, the percentage of cells in S phase from CR-LM was significantly greater ($**P < .01$) than the control.

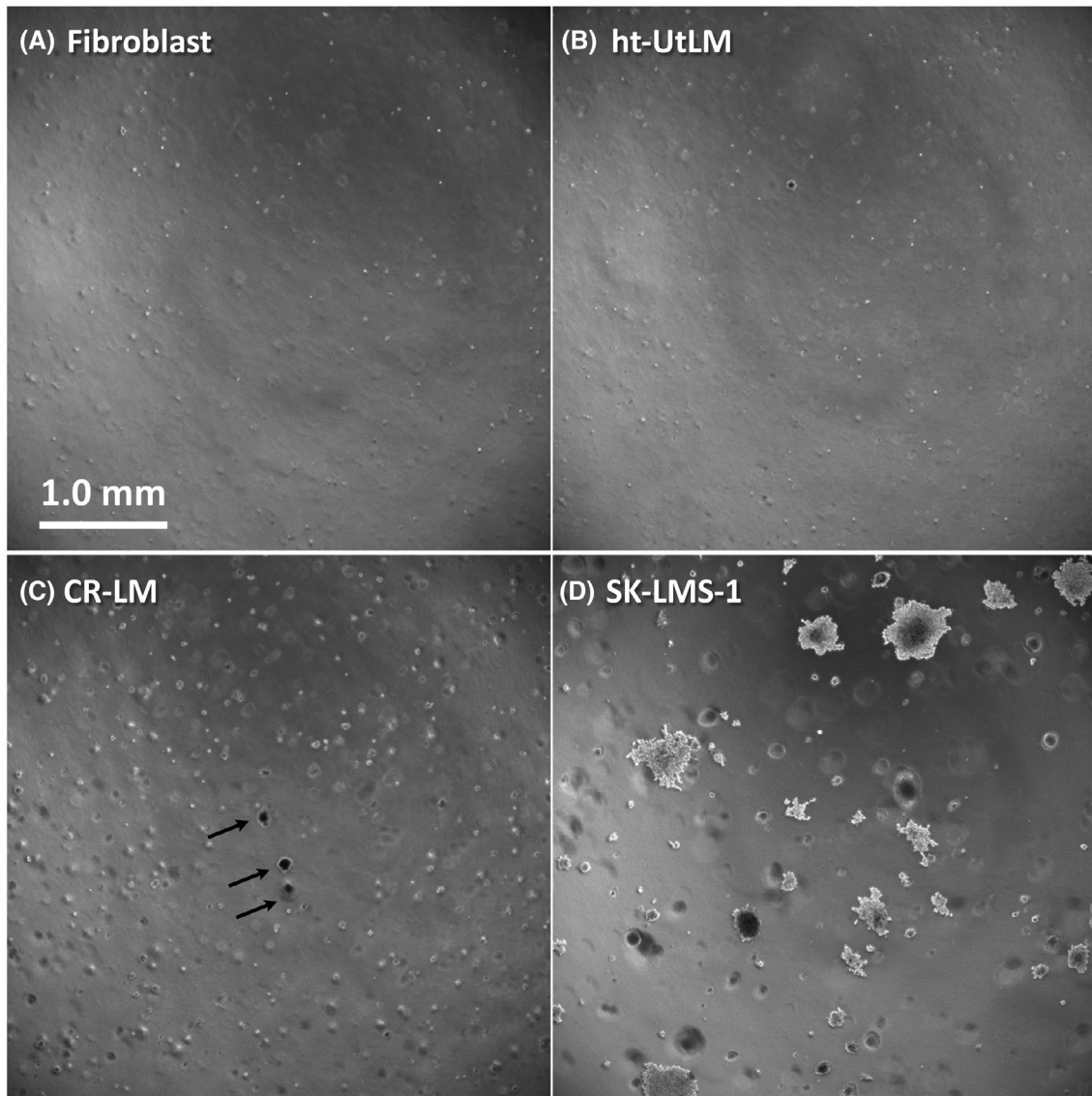


FIGURE 3 Soft agar assays to assess anchorage-independent growth. A, Fibroblast cells served as negative controls. B, Ht-UtLM cells. C, CR-LM, the viable colonies are indicated by arrows. D, SK-LMS-1 cells served as positive controls. Images acquired by epifluorescence microscopy in phase contrast mode. A-D, (scale bar = 1 mm)

3.3 | Cd exposure promoted anchorage-independent growth and cell migration

Soft agar assays were conducted to evaluate whether Cd exposure would promote anchorage-independent growth. Fibroblast (negative control), ht-UtLM, CR-LM, and SK-LMS-1 (human vulvar leiomyosarcoma, positive control) cells were tested for their ability to grow in soft agar (Figure 3). After growing in soft agar for 3 weeks, neither fibroblast or ht-UtLM cells developed viable colonies (Figure 3A,B). Multiple viable small colonies were detected in CR-LM (Figure 3C). As expected, SK-LMS-1 cells developed multiple viable larger colonies (Figure 3D). These findings suggest that CR-LM has acquired the ability to grow independently of being anchored.

As illustrated by full track visualization, 8-week Cd exposure accelerated CR-LM cell motility (Figure 4A,B). Quantitative cell migration analysis was done by tracking individual nuclei with Imaris. As shown in the histograms of track length distributions in Figure 4C,D, there were 319 and 747 ht-UtLM and CR-LM cells, respectively, which passed the threshold of the tracking parameters. In ht-UtLM, the top 3 fast-moving cells fell into the bin at 175 μm , and the peak was located at the bin at 45 μm (Figure 4C). Whereas in CR-LM, the fastest moving cell fell into the bin at 285 μm , and the peak was positioned at 65 μm (Figure 4D). The average migration distance (track length) for the control was 54.15 μm with SD 31.06 μm , whereas the average migration distance for CR-LM was 88.25 μm with SD 43.70 μm (Figure 4C,D). To show normalized distributions, an R density function was used to plot the probability density for both populations

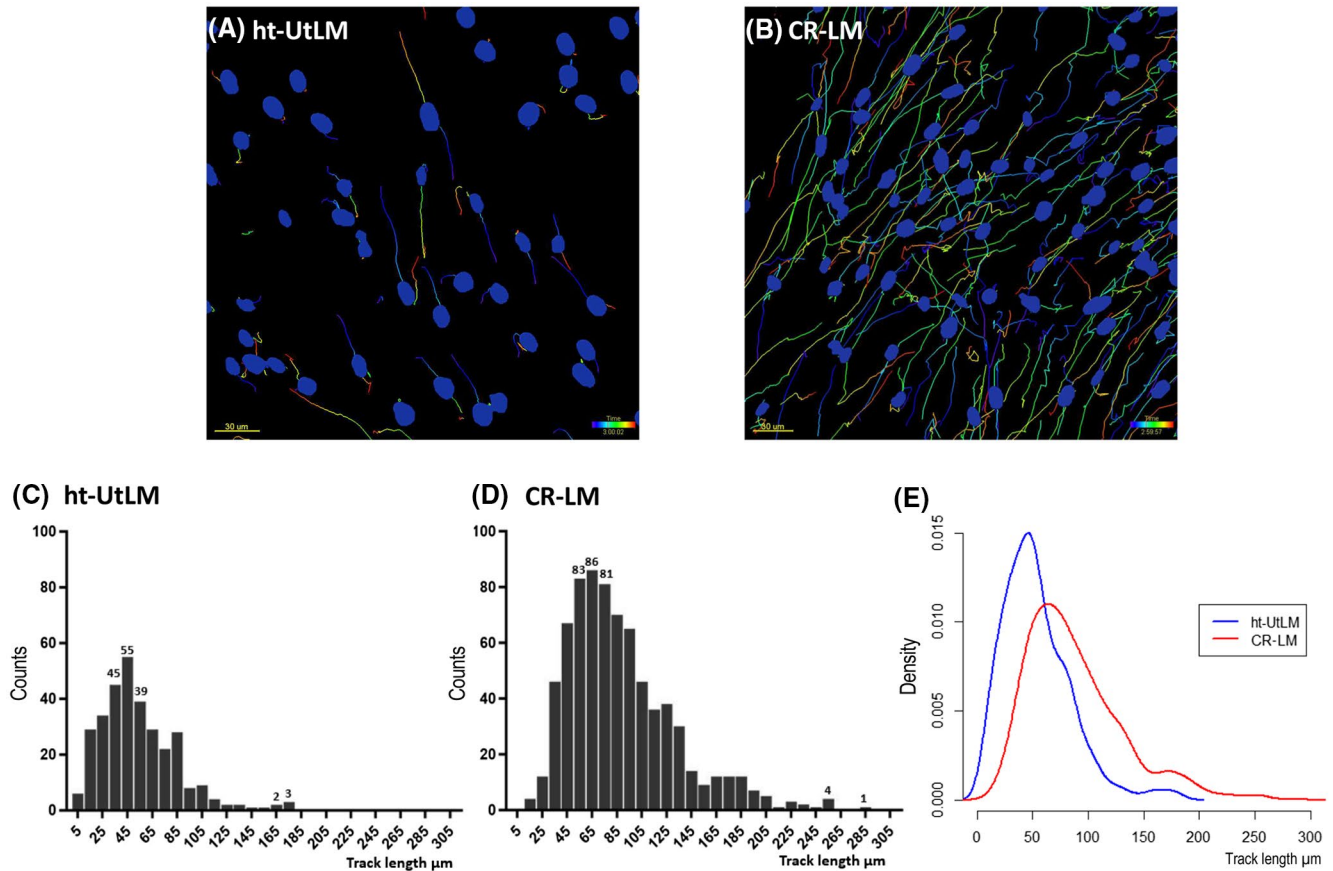


FIGURE 4 Prolonged Cd exposure stimulated cell motility in CR-LM cells. A and B, The full track visualization of time-lapse experiments for ht-UtLM (A) and CR-LM (B) cells, respectively. C and D, Frequency distribution of the track length values for ht-UtLM (C) and CR-LM (D) cells as shown in the histograms. E, The superimposed track length distributions of ht-UtLM and CR-LM cells by probability density plotted by density function with RStudio.

(Figure 4E). The one-tailed t-test with a two-sample unequal variance returned a P -value of $1.34E-42$, indicating that CR-LM cells had significantly greater motility than ht-UtLM controls.

3.4 | Differential gene expression induced by Cd exposure

There were 580 and 600 codesets for PanCancer Pathways and Progression Panels, respectively, with 132 overlapping codesets. The data discussed in this publication have been deposited in NCBI's Gene Expression Omnibus²⁰ and are accessible through GEO Series accession number GSE161456 (<https://www.ncbi.nlm.nih.gov/geo/query/acc.cgi?acc=GSE161456>). For CR-LM and control cells, after applying a fold-change filter (cutoff at 2.0), there were 180 DEGs (Dataset S1). The RCC (Recorder Code Counts) files derived from the two panels were imported into nSolver to display overall gene expression profile in volcano plot (Figure 5A). The top up-regulated DEG in CR-LM was *SPPI*, and the top down-regulated DEG was *SULF1* (Figure 5A). Interestingly, both *SPPI* and *SULF1* genes encode matricellular proteins that exist in

ECM and serve as non-structural regulatory proteins. The matricellular proteins modulate cell function by interacting with cell-surface receptors, proteases, hormones, and other bioeffector molecules, as well as with structural matrix proteins. In CR-LM, many genes encoding for ECM constitutive components were significantly downregulated. The genes encoding for collagens such as *COL1A1*, *COL3A1*, *COL5A2*, *COL5A1*, *COL4A1*, *COL1A2*, *COL6A1*, *COL4A2*, *COL11A1*, and *COL18A1* were all reduced ranging from approximately 2- to nearly 10-fold (Table 1). Additionally, genes encoding for fibronectin and laminins, also primary high-molecular weight glycoproteins of ECM, were downregulated ranging from 3.55- to 4.49-fold. The members of SLRP family, such as *LUM*, *BGN*, *DCN*, and *FMOD*, were downregulated 22.22-, 9.06-, 2.39-, and 2.58-fold, respectively. Also, *THBS1*, a gene encoding an adhesive glycoprotein in ECM that can bind to collagen, laminin, and fibronectin and mediates cell-matrix interactions, was downregulated more than 40-fold (Table 1). However, genes encoding for MMPs were significantly upregulated. For example, the transcript of *MMP1*, *MMP3*, and *MMP10* were upregulated by 26.35-, 6.71-, and 4.22-fold, respectively.

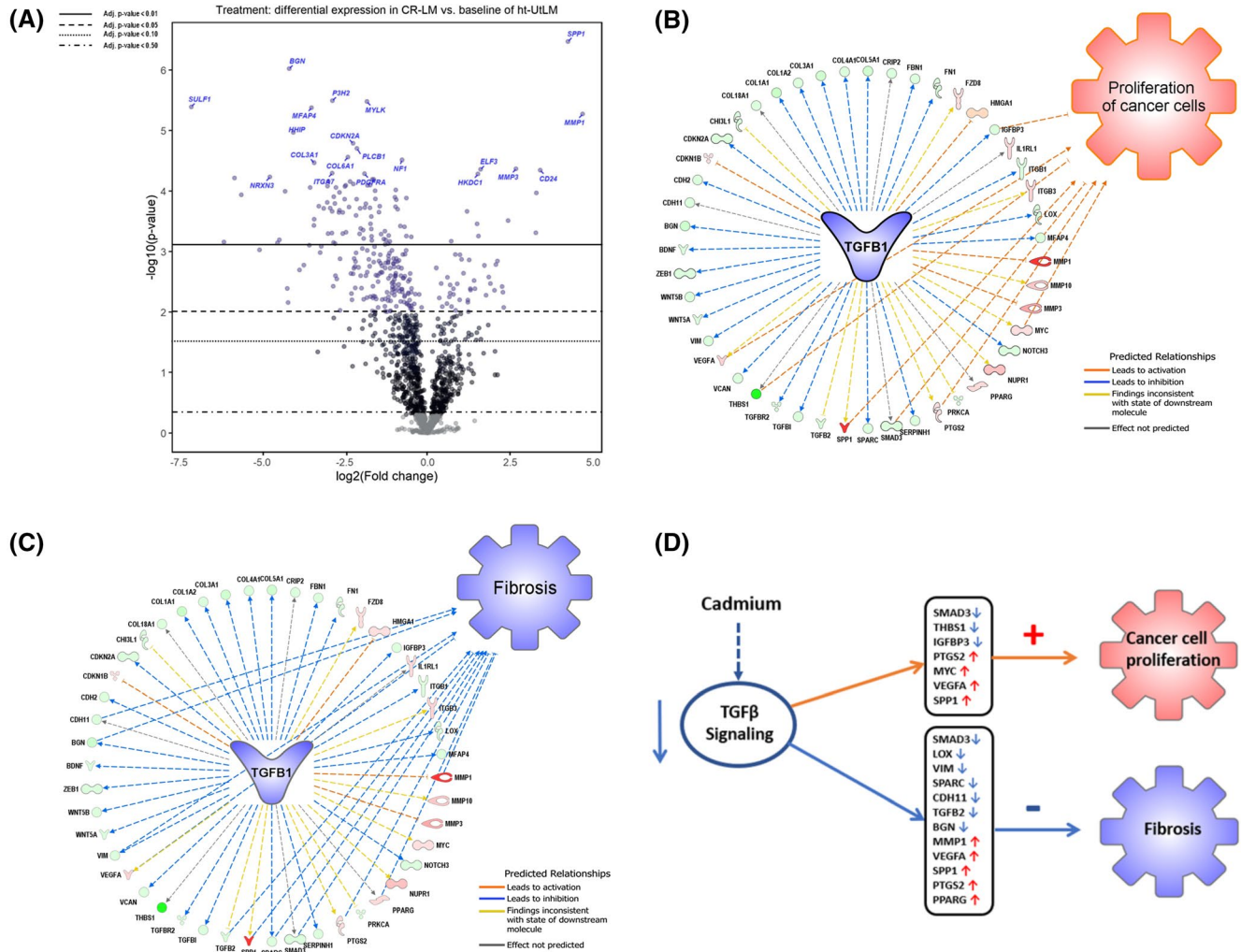


FIGURE 5 Cd exposure induced differentially expressed genes and signaling pathway changes. A, Volcano plot of altered gene expression patterns in Cd-exposed CR-LM cells. The volcano plot shows each gene's $-\log_{10}(P\text{-value})$ and \log_2 fold change with the chosen covariate. Highly significant genes fall at the top of the plot and those genes highly and differentially expressed fall to either side. The horizontal lines indicate different false discovery rate (FDR) thresholds. Genes are colored if the resulting P -value is below the given FDR threshold. The 20 most statistically significant genes are labeled. B, IPA predicted that the inhibited TGFB1 signaling favored cancer cell proliferation. Among the 47 nodes (molecules) within the TGFB1 network, seven relationship lines were identified to be associated with activation of cancer cell proliferation. The nodes implicated as having proliferative stimulatory effects (orange lines) were *SPP1*, *MYC*, *VEGFA*, *PTGS2*, *IGFBP3*, *SMAD3*, and *THBS1*. C, IPA predicted that the inhibited TGFB1 signaling in CR-LM suppressed fibrosis. Among the 47 nodes within the TGFB1 network, 12 relationship lines were identified to be associated with the suppression of fibrosis. The nodes implicated as having an inhibitory effect (blue lines) were *MMP1*, *LOX*, *CDH1*, *BGN*, *VIM*, *VEGFA*, *TGFB2*, *SPP1*, *SPARC*, *SMAD3*, *PTGS2* and *PPARG*. D, IPA analysis predicted that Cd exposure inhibits TGFB signaling, promotes cell proliferation, and inhibits fibrosis

3.5 | Cd exposure resulted in TGFB signaling inhibition

Based on IPA analysis of NanoString datasets, *TGFB1* was identified to be the top upstream regulator being significantly inhibited with an activation z -score of -2.75 and P -value of $4.87E-29$ (Dataset S2). *TGFB* genes encode secreted ligands of TGFB superfamily. Ligands of this family bind to various TGFB receptors leading to recruitment and activation of SMAD family transcription factors. In

our IPA dataset, *TGFB2* and *TGFB2R* molecules involved in early events of TGFB signaling were downregulated by 6.85- and 2.18-fold (Dataset S2). *SMAD3*, a regulator in TGFB signaling and downstream of TGFB receptor, was downregulated 2.50-fold. Notably, *THBS1*, a major TGFB ligand activator, was downregulated by 41.99-fold (Dataset S2), which may have contributed to the inhibition of TGFB signaling. To directly visualized barcode counts for critical genes in TGFB signaling, we generated boxplots based on RCC files. As shown in Figure S1,

Symbol	Entrez gene name	Expr FDR (q-value)	Expr fold change	Location
<i>MMP1</i>	Matrix metalloproteinase 1	2.03E-06	26.35	Extracellular space
<i>MMP3</i>	Matrix metalloproteinase 3	1.07E-05	6.71	Extracellular space
<i>MMP10</i>	Matrix metalloproteinase 10	1.48E-02	4.22	Extracellular space
<i>COL1A1</i>	Collagen type I alpha 1 chain	5.41E-04	-9.94	Extracellular space
<i>COL3A1</i>	Collagen type III alpha 1 chain	7.52E-06	-8.55	Extracellular space
<i>COL5A2</i>	Collagen type V alpha 2 chain	1.04E-04	-8.51	Extracellular space
<i>COL5A1</i>	Collagen type V alpha 1 chain	2.66E-04	-8.49	Extracellular space
<i>COL4A1</i>	Collagen type IV alpha 1 chain	7.05E-05	-5.33	Extracellular space
<i>COL1A2</i>	Collagen type I alpha 2 chain	5.96E-04	-4.37	Extracellular space
<i>COL6A1</i>	Collagen type VI alpha 1 chain	8.02E-04	-3.40	Extracellular space
<i>COL4A2</i>	Collagen type IV alpha 2 chain	2.44E-04	-2.77	Extracellular space
<i>COL11A1</i>	Collagen type XI alpha 1 chain	1.64E-04	-2.68	Extracellular space
<i>COL18A1</i>	Collagen type XVIII alpha 1 chain	1.99E-04	-2.46	Extracellular space
<i>FNI</i>	Fibronectin 1	2.50E-02	-3.55	Extracellular space
<i>LAMA3</i>	Laminin subunit alpha 3	1.39E-03	-3.80	Extracellular space
<i>LAMA4</i>	Laminin subunit alpha 4	7.05E-05	-4.49	Extracellular space
<i>LUM</i>	Lumican	4.96E-07	-22.22	Extracellular space
<i>BGN</i>	Biglycan	1.07E-05	-9.06	Extracellular space
<i>FMOD</i>	Fibromodulin	2.85E-07	-2.58	Extracellular space
<i>DCN</i>	Decorin	1.66E-03	-2.39	Extracellular space
<i>THBS1</i>	Thrombospondin 1	1.85E-04	-41.99	Extracellular space

TABLE 1 Differential expression of extracellular and metalloproteinase genes in CR-LM and ht-UtLM cells

Note: This table was derived from IPA Canonical Pathway analysis on combined Cancer Progression and Cancer Pathways panels.

Pink = Upregulated gene expression fold changes; Green = Downregulated gene expression fold changes.

the barcode counts for *SMAD3*, *TGFB2*, *TGFB3*, and *TGFB2* were all suppressed in CR-LM.

3.6 | The inhibition of TGFB signaling promotes cancer cell proliferation and inhibits fibrosis

IPA revealed that the inhibited TGFB pathway was associated with enhanced cancer cell proliferation (Figure 5B). In TGFB1 network, 14 relationship lines were found to be associated with

cancer cell proliferation. Among the 14 relationship lines, there were seven orange lines (leading to activation), five yellow (inconsistent prediction), two black (effect not predicted), and zero blue (leading to inhibition). For the sake of clarity, the yellow, black, and blue lines are not shown in Figure 5B. The seven nodes associated with enhanced proliferation were: 1. *SPP1*; 2. *VEGFA*; 3. *PTGS2*; 4. *MYC* (MYC proto-oncogene bHLH transcription factor); 5. *IGFBP3* (insulin-like growth factor binding protein 3); 6. *SMAD3*; and 7. *THBS1*. The Cd exposure mediated expression of the seven genes (orange lines) aligned with the expression direction of the same molecules

in Ingenuity Knowledge Base for cancer cell proliferation. It was therefore strongly suggested that long-term Cd exposure would render fibroid cells to be more proliferative (Figure 5B, Dataset S2). IPA also revealed that the inhibited TGFB1 signaling was responsible for decreased fibrosis (Dataset S2, Figure 5C). In TGFB1 network, 21 relationship lines were found to be associated with fibrosis. There were zero orange, four yellow, five gray, and 12 blue lines. For the sake of clarity, only the blue lines were displayed. The 12 nodes directly associated with the suppressed fibrosis were 1. *CDH11* (cadherin 11); 2. *BGN*; 3. *VIM* (vimentin); 4. *VEGFA*; 5. *TGFB2* (transforming growth factor β 2); 6. *SPP1*; 7. *SPARC* (secreted protein acidic and cysteine rich); 8. *SMAD3*; 9. *PTGS2*; 10. *PPARG* (peroxisome proliferator activated receptor γ); 11. *MMPI*; and 12. *LOX* (lysyl oxidase). IPA analysis predicted that Cd exposure inhibits TGFB signaling, promotes cell proliferation, and decreases fibrosis (Figure 5D).

3.7 | Confirmation of NanoString data with protein array and confocal microscopy

We stained the fibroid cells with collagen 1 and fibronectin antibodies to visualize expression of these major ECM proteins. As illustrated in Figure 6A-D, both collagen and fibronectin protein expression were reduced in CR-LM cells; however, COL1A1 was mostly localized in the cytoplasm, and fibronectin was mostly expressed along the cell surface of ht-UtLM cells. Additionally, a human MMP antibody protein array was used to quantify MMP protein levels in cell extracts. As shown in Figure 6E-H, the levels of MMP1, MMP3, and MMP10 in protein array blots were all increased in CR-LM. Further densitometric quantification showed that the expression of MMP1, MMP3, and MMP10 was upregulated by 32.4-, 4.8-, and 4.5-fold, respectively (P -value < .0001). The strong correlation between NanoString results and the protein

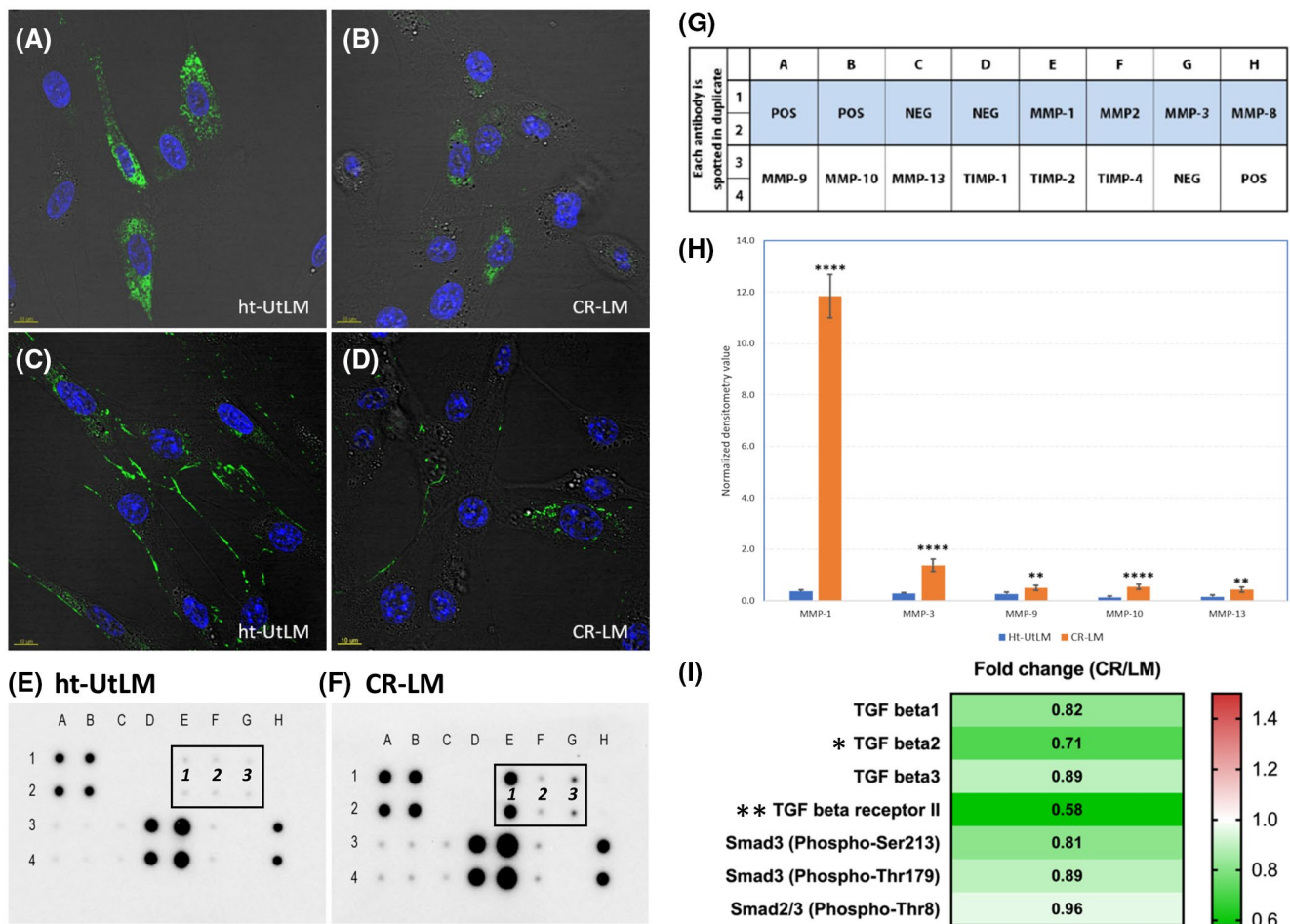


FIGURE 6 Prolonged Cd exposure reduced the protein expression of collagen 1 and fibronectin and increased MMPs. A and B, COL1A1 expression in ht-UtLM and CR-LM cells. C and D, Fibronectin expression in ht-UtLM and CR-LM cells. E, MMPs and TIMPs protein expression profile of ht-UtLM. The positions of MMP1, MMP2, and MMP3 are denoted as 1, 2, and 3. F, CR-LM expression profile. G, The array layout. H, Histogram of normalized signal intensity for significantly expressed MMPs. The protein expression profiles were acquired with RayBio C-Series Human Matrix Metalloproteinase Antibody Array C1. The signal intensity for each protein was normalized with Image J. I, Decreased expression of TGF β signaling proteins following continuous Cd exposure detected by TGF β phospho-antibody array. * P < .05; ** P < .01; **** P < .0001

expression data suggests that the NanoString platform is robust and reliable.

We investigated the protein expression and phosphorylation levels of critical proteins in TGF β signaling pathway using a TGF β phospho antibody array. In accordance with our NanoString data, the expression of TGF β 1, TGF β 2, TGF β 3, and TGF β receptor II was all decreased in CR-LM cells (Figure 6I). Additionally, the phosphorylation levels of SMAD3 (phospho-Ser213 and phospho-Thr179) and SMAD2/3 (Phospho-Thr8) were also decreased. However, only fold changes for TGF β 2 ($P < .05$) and TGF β receptor 2 ($P < .01$) were statistically significant. Overall, the direction of the expression changes in these critical proteins in TGF β signaling detected by the TGF β phospho antibody array reinforces that prolonged Cd exposure inhibits TGF β signaling.

4 | DISCUSSION

The effects of prolonged Cd exposure on phenotypic and signaling pathway changes in human uterine fibroid cells were investigated in this study. Our results showed that Cd exposure altered fibroid cell morphology, increased cell proliferation, induced anchorage-independent growth, and enhanced cell motility. When fibroid cells were maintained in Cd-containing medium for 8 weeks, a subset of the once severely stressed cells developed into fast-growing Cadmium-Resistant Leiomyoma (CR-LM) cultures. Previous studies indicated that Cd and Cd-containing compounds have carcinogenic potential in experimental animals and humans.²¹ It is therefore no surprise that Cd exposure could induce morphological changes and the formation of focal aggregates showing a proclivity towards cancer progression.

Long-term Cd exposure significantly upregulated Ki-67 expression and enhanced cell proliferation. We reported earlier that ht-UtLM cells are highly proliferative following short-term Cd exposures.^{13,14} Ki-67 is a proliferation marker, expressed in all active phases of the cell cycle (G1, S, G2, and mitosis), but absent in quiescent phase. Cd exposure significantly altered the cell cycle, with the percentage of cells in G2/M phase being increased in CR-LM cells. The higher percentage of cells in G2/M correlated well with the increased Ki-67 expression in CR-LM cells. Moreover, the abundance of peripheral deposits of cytoplasmic glycogen granules suggested increased glycogen reserves for possible increased cell motility and proliferation.²² Cancer cells under aerobic conditions consume more glucose than required for ATP generation via oxidative phosphorylation, a phenomenon known as the Warburg effect.^{22,23}

AIG (Anchorage-independent growth) is the ability of transformed cells to grow independently of a solid surface and is one of the hallmarks of cancer cells. The acquisition of AIG is thought to be a crucial step for malignancy to allow

cells to metastasize, colonize in other tissues, and grow at distant sites.²⁴ Previously, we demonstrated that ht-UtLM cells do not show AIG and fail to produce viable colonies in soft agar.¹⁶ In this study, CR-LM developed multiple viable colonies in soft agar, which would suggest that CR-LM cells have acquired AIG characteristics and are progressing towards a cancer phenotype. Overexpression of ECM component, lumican, in melanoma cells has been reported to inhibit AIG in agarose gel and the capacity to invade the extracellular matrix.²⁵ In our dataset, lumican expression was inhibited by 22-fold (Table 1), suggesting that lumican downregulation may have been a contributor to AIG in CR-LM. Also, prolonged Cd exposure significantly increased CR-LM cell motility. Metastatic cancer cells undergo dramatic remodeling of ECM and cytoskeletal network and display enhanced migration.²⁶ The significant upregulation of multiple matrix metalloproteinases and the significant downregulation of ECM components such as lumican, fibronectin, and collagen may all contribute to the enhanced motility.

In the NanoString dataset, genes encoding for ECM components (collagens, fibronectin, laminin, and proteoglycans) were inhibited significantly. In the volcano plot, the top differentially expressed genes (such as *SULF1*, *LUM*, *BGN*, *SPP1*, and *MMPI1*) were all regulators or components of the ECM and thought to be important in cancer progression and metastasis. Downregulation of *SULF*²⁷ and *LUM* gene expression in breast cancer is associated with rapid cancer progression and poor survival.²⁵ The multiple structural components of the ECM have been reported to prevent invasion of cancer cells and possesses an intrinsic mechanism to downregulate signaling processes that are required for cancer cell proliferation. Small Leucine Rich Proteoglycans (SLRPs) such as LUM, BGN, DCN, and FMOD are ubiquitous ECM components involved in matrix structural organization and as such can potentially regulate cancer cell multiplication, angiogenesis and migration.²⁸ In breast cancer, it was shown that the presence of laminins in ECM is critical for healthy breast cells to form organized clusters *in vitro* that resemble breast glands. In the absence of laminins, however, the communication between the breast cells and ECM is lost, and the healthy breast cells become disorganized and start to form clumps that resemble tumors, which highlights the importance of laminins and other ECM components in maintaining the differentiated state.²⁹ It was shown that LUM has a direct role in regulating cancer progression. For example, reduced LUM expression in breast cancer is associated with rapid cancer progression and poor survival. On the other hand, high levels of LUM significantly suppressed subcutaneous tumor formation in a syngeneic mouse model.²⁵ Both DCN and LUM may be considered anti-tumor factors due to their roles in negative regulation of tumor cell proliferation. Therefore, in CR-LM top differentially expressed genes

identified in a volcano plot suggested a direction towards cancer progression. Interestingly, *MMP* genes, which are responsible for degrading ECM components, were highly overexpressed in CR-LM. It is worth noting that the predominant role of MMPs is to mobilize growth factors and cytokines by dissociating them from the ECM.³⁰

There are more than 560 putative proteases in the human degradome that are responsible for the irreversible post-translational modifications, with MMPs as key nodal proteases. The MMPs directly regulated a host of signaling molecules, including most of the 54 chemokines in human.^{31,32} Elevated expression of MMP1 is closely associated with lymph node metastasis in patients with advanced cervical cancer.³³ Interestingly, Cd exposure not only significantly increased MMP1 transcript levels by as much as 26.35-fold but also boosted MMP1 protein expression level by 32.4-fold in CR-LM cells. Additionally, the Cd exposure dramatically suppressed transcript and protein expression levels of ECM structural components such as fibronectin and collagens. The differential alterations in the MMP and ECM expression might greatly contribute to the Cd-mediated cellular proliferation and migration stimulation.

The node TGF β 1 was identified as the top upstream regulator being significantly inhibited in CR-LM cells. The biological and physiological functions of TGF β ligands and receptors are of critical importance in human diseases. TGF β signaling has been implicated as one of the major players in uterine fibroid pathophysiology that mediates cellular migration, fibroid growth, and metabolism. The upregulation of TGF β signaling in uterine fibroids results in excessive extracellular matrix production and accumulation.³⁴ This excessive overexpression of TGF β may be responsible for clinically symptomatic uterine fibroids.³⁴ Importantly, genetic studies have consistently demonstrated that TGF β signaling serves as a tumor suppressor and plays a critical role in preventing carcinogenesis in normal epithelial cells.³⁵ The tumor suppressive effects of TGF β in normal epithelial cells include cell cycle arrest, apoptosis, and prevention of cell immortalization. In CR-LM, the major TGF β ligand activator *THBS1* was downregulated more than 40-fold (Dataset S1, Table 1), which could contribute to the inhibition of TGF β signaling. The modulation of *THBS1* activity may represent a novel approach to selectively regulate TGF β signaling in fibrotic disease.³⁶ The prolonged Cd exposure significantly attenuated TGF β signaling, which might compromise the tumor suppressive activities of TGF β and thereby favor pro-cancer events.

Based on the direction of the gene expression changes of downstream nodes (molecules), IPA predicted significant inhibition of the TGF β 1 pathway. Our TGF β protein array data confirmed decreased expression of TGF β 1, TGF β 2, TGF β 3, and TGF β R2, all major TGF β signaling proteins in CR-LM cells exposed to Cd for 2 months.

However, it should be noted that in the protein phosphorylation array analysis, all the fold-change values were marginal although TGF β 2 and TGF β R2 were significant. The TGF β ligand is a multifunctional cytokine that signals to nucleus through cell surface transmembrane receptors with serine/threonine kinase activity and cytoplasmic effectors, including SMAD proteins. Many members of the SLRP family such as decorin, biglycan, asporin, and fibromodulin are able to bind to and modulate TGF β pathways. Moreover, decorin modulates the TGF β pathway and regulates matrix organization and mechanical characteristics of three-dimensional collagen matrices.³⁷ Multiple lines of evidence suggest that both lumican and decorin inhibit cancer proliferation and invasion and are considered as anti-tumor factors. Decorin has been implicated in the negative regulation of tumor cell proliferation via interaction with TGF β signaling network.²⁵ In our dataset, the significant downregulation of *SLRP* transcripts aligned well with the predicted inhibition of TGF β signaling.

In summary, prolonged Cd exposure rendered fibroid cells morphologically distinctive, anchorage-independent, and highly proliferative. Our data strongly suggest that the Cd induced phenotypic characteristics and dysregulated gene expression patterns in fibroid cells are indicative of progression from a benign cell type producing excessive amounts of ECM components towards a proliferative cancerous phenotype. Further studies are required to assess whether long-term environmental Cd exposures pose a health hazard for woman with benign uterine fibroids.

ACKNOWLEDGMENTS

The authors thank Dr Agnes Janoshazi, Fluorescence Microscopy and Imaging Center; Dr Carl Bortner and Ms Maria Sifre, Flow Cytometry Center; Ms Deloris Sutton, Electron Microscopy Core; Ms Natasha Clayton and Ms Heather Jensen, Immunohistochemistry Core, and Mr Trey Saddler, Office of Data Science for their excellent technical support. This research was supported by the Intramural Research Program of the NIEHS and DNTP (ES021196-27).

CONFLICT OF INTEREST

All authors declare that they have no competing interests.

AUTHOR CONTRIBUTIONS

All authors have read and approved the manuscript. Y. Yan participated in design of the research, performed experiments, analyzed data, and wrote manuscript; J. Liu, A. Lawrence, M.J. Dykstra, R. Fannin, K. Gerrish, C.J. Tucker, E. Scappini conducted experiments and analyzed data; D. Dixon designed research and wrote manuscript.

ORCID

Darlene Dixon  <https://orcid.org/0000-0002-7001-2985>

REFERENCES

- Ye S, Chung HW, Jeong K, et al. Blood cadmium and volume of uterine fibroids in premenopausal women. *Ann Occup Environ Med.* 2017;29:22. <https://doi.org/10.1186/s40557-017-0178-8>.
- Baird DD, Dunson DB, Hill MC, Cousins D, Schectman JM. High cumulative incidence of uterine leiomyoma in black and white women: ultrasound evidence. *Am J Obstet Gynecol.* 2003;188:100-107.
- Luevano J, Damodaran C. A review of molecular events of cadmium-induced carcinogenesis. *J Environ Pathol Toxicol Oncol.* 2014;33:183-194.
- Nogawa K, Honda R, Yamada Y, et al. Critical concentration of cadmium in kidney cortex of humans exposed to environmental cadmium. *Environ Res.* 1986;40:251-260.
- Satarug S. Dietary cadmium intake and its effects on kidneys. *Toxics.* 2018;6(1):15. <https://doi.org/10.3390/toxics6010015>.
- Elinder C-G. Normal values for cadmium in human tissues, blood, and urine in different countries. In: Friberg L, Elinder C-G, Kjellstrom T, Nordberg GF, eds. *Cadmium and Health: A Toxicological and Epidemiological Appraisal Volume 1: Exposure, Dose, and Metabolism.* Vol. 1. Boca Raton, FL: CRC Press, Inc.; 1985:81-102.
- Rafati Rahimzadeh M, Rafati Rahimzadeh M, Kazemi S, Moghadamnia AA. Cadmium toxicity and treatment: an update. *Caspian J Intern Med.* 2017;8:135-145.
- Järup Lars, Åkesson Agneta. Current status of cadmium as an environmental health problem. *Toxicol. Appl. Pharmacol.* 2009;238(3):201-208. <https://doi.org/10.1016/j.taap.2009.04.020>.
- Johnson MD, Kenney N, Stoica A, et al. Cadmium mimics the in vivo effects of estrogen in the uterus and mammary gland. *Nat Med.* 2003;9:1081-1084.
- Stoica A, Katzenellenbogen BS, Martin MB. Activation of estrogen receptor-alpha by the heavy metal cadmium. *Mol Endocrinol.* 2000;14:545-553.
- Ali I, Penttinen-Damdimopoulou PE, Mäkelä SI, et al. Estrogen-like effects of cadmium in vivo do not appear to be mediated via the classical estrogen receptor transcriptional pathway. *Environ Health Perspect.* 2010;118:1389-1394.
- Liu Z, Yu X, Shaikh ZA. Rapid activation of ERK1/2 and AKT in human breast cancer cells by cadmium. *Toxicol Appl Pharmacol.* 2008;228:286-294.
- Gao X, Yu L, Moore AB, Kissling GE, Waalkes MP, Dixon D. Cadmium and proliferation in human uterine leiomyoma cells: evidence of a role for EGFR/MAPK pathways but not classical estrogen receptor pathways. *Environ Health Perspect.* 2015;123:331-336.
- Liu J, Yu L, Castro L, et al. A nongenomic mechanism for “metalloestrogenic” effects of cadmium in human uterine leiomyoma cells through G protein-coupled estrogen receptor. *Arch Toxicol.* 2019;93:2773-2785.
- Pollack AZ, Ranasinghe S, Sjaarda LA, Mumford SL. Cadmium and reproductive health in women: a systematic review of the epidemiologic evidence. *Curr Environ Health Rep.* 2014;1:172-184.
- Carney SA, Tahara H, Swartz CD, et al. Immortalization of human uterine leiomyoma and myometrial cell lines after induction of telomerase activity: molecular and phenotypic characteristics. *Lab Invest.* 2002;82:719-728.
- Yan Y, Yu L, Castro L, Dixon D. ER α 36, a variant of estrogen receptor α , is predominantly localized in mitochondria of human uterine smooth muscle and leiomyoma cells. *PLoS ONE.* 2017;12:e0186078.
- Dykstra MJ. Why 4F:1G fixative works for me. *Microscopy Today.* 2010;18:50-53.
- Castro L, Gao X, Moore AB, et al. A high concentration of genistein induces cell death in human uterine leiomyoma cells by autophagy. *Expert Opin Environ Biol.* 2016;5(Suppl 1). <https://doi.org/10.4172/2325-9655.S1-003>.
- Edgar R, Domrachev M, Lash AE. Gene expression omnibus: NCBI gene expression and hybridization array data repository. *Nucleic Acids Res.* 2002;30:207-210.
- Waalkes MP, Rehm S. Chronic toxic and carcinogenic effects of cadmium chloride in male DBA/2Ncr and NFS/NCr mice: strain-dependent association with tumors of the hematopoietic system, injection site, liver, and lung. *Fundam Appl Toxicol.* 1994;23:21-31.
- Zois CE, Harris AL. Glycogen metabolism has a key role in the cancer microenvironment and provides new targets for cancer therapy. *J Mol Med.* 2016;94:137-154.
- Lu J. The Warburg metabolism fuels tumor metastasis. *Cancer Metastasis Rev.* 2019;38:157-164.
- Guadamillas MC, Cerezo A, Del Pozo MA. Overcoming anoikis-pathways to anchorage-independent growth in cancer. *J Cell Sci.* 2011;124:3189-3197.
- Naito Z. Role of the small leucine-rich proteoglycan (SLRP) family in pathological lesions and cancer cell growth. *J Nippon Med Sch.* 2005;72:137-145.
- Yilmaz M, Christofori G. Mechanisms of motility in metastasizing cells. *Mol Cancer Res.* 2010;8:629-642.
- Lai JP, Sandhu DS, Shire AM, Roberts LR. The tumor suppressor function of human sulfatase 1 (SULF1) in carcinogenesis. *J Gastrointest Cancer.* 2008;39:149-158.
- Appunni S, Anand V, Khandelwal M, Gupta N, Rubens M, Sharma A. Small leucine rich proteoglycans (decorin, biglycan and lumican) in cancer. *Clin Chim Acta.* 2019;491:1-7.
- Furuta S, Ren G, Mao JH, Bissell MJ. Laminin signals initiate the reciprocal loop that informs breast-specific gene expression and homeostasis by activating NO, p53 and microRNAs. *eLife.* 2018;7:e26148. <https://doi.org/10.7554/eLife.26148>.
- Pardo A, Selman M. MMP-1: the elder of the family. *Int J Biochem Cell Biol.* 2005;37:283-288.
- Puente XS, Sánchez LM, Overall CM, López-Otín C. Human and mouse proteases: a comparative genomic approach. *Nat Rev Genet.* 2003;4:544-558.
- Overall CM, Kleifeld O. Tumour microenvironment—opinion: validating matrix metalloproteinases as drug targets and anti-targets for cancer therapy. *Nat Rev Cancer.* 2006;6:227-239.
- Tian R, Li X, Gao Y, Li Y, Yang P, Wang K. Identification and validation of the role of matrix metalloproteinase-1 in cervical cancer. *Int J Oncol.* 2018;52:1198-1208.
- Ciebiera M, Włodarczyk M, Wrzosek M, et al. Role of transforming growth factor β in uterine fibroid biology. *Int J Mol Sci.* 2017;18(11):2435. <https://doi.org/10.3390/ijms18112435>.
- Lebrun JJ. The dual role of TGF β in human cancer: from tumor suppression to cancer metastasis. *ISRN Mol Biol.* 2012;2012:381428.
- Murphy-Ullrich JE, Suto MJ. Thrombospondin-1 regulation of latent TGF- β activation: a therapeutic target for fibrotic disease. *Matrix Biol.* 2018;68-69:28-43.

37. Schaefer L, Iozzo RV. Biological functions of the small leucine-rich proteoglycans: from genetics to signal transduction. *J Biol Chem*. 2008;283:21305-21309.

SUPPORTING INFORMATION

Additional Supporting Information may be found online in the Supporting Information section.

How to cite this article: Yan Y, Liu J, Lawrence A, et al. Prolonged cadmium exposure alters benign uterine fibroid cell behavior, extracellular matrix components, and TGF β signaling. *The FASEB Journal*. 2021;35:e21738. <https://doi.org/10.1096/fj.202100354R>